A Simple F–Test Based Spectrum Sensing Technique for MIMO Cognitive Radio Networks

Tilahun M. Getu[†‡], Wessam Ajib[‡], and René Jr. Landry[†]
[†]École de Technologie Supérieure (ÉTS), Montréal, QC, Canada
[‡]Université du Québec à Montréal (UQÀM), Montréal, QC, Canada
tilahun-melkamu.getu.1@ens.etsmtl.ca, ajib.wessam@uqam.ca, and renejr.landry@etsmtl.ca

***Abstract*—An F–test detector with a simple analytical false alarm threshold expression is considered an alternative to the blind detectors which exhibit complicated analytical expressions. Proposed for a single-input multiple-output (SIMO) systems, the existing F–test requires the channel state information (CSI) as a prior knowledge. On the contrary, the CSI requirement renders a sensitivity to a CSI estimation error and multiple-input multiple-output (MIMO) systems guarantee better array gain, spatial diversity gain, spatial multiplexing gain, and interference reduction than SIMO systems. Accordingly, we present and evaluate the performance of a simple F–test based spectrum sensing technique that doesn't require the knowledge of the CSI for the MIMO cognitive radio networks. For this detector, exact and asymptotic analytical performance closed-form expressions are derived. Simulations assess the performance of the presented detector and validate the derived closed-form expressions.**

***Index Terms*—Cognitive radio, F–test, SIMO systems, MIMO systems, cognitive radio networks.**

I. Introduction

A. Related Works

In order to overcome the discrepancy between spectrum scarcity—which is getting aggravated by an ever-increasing demand for higher data rates—and spectrum underutilization, cognitive radio (CR) has emerged as a promising technology. As an enabler to this technology which underpins a vision regarding spectrum sharing, spectrum sharing techniques named as *spectrum underlay* and *spectrum overlay* have been proposed [1], [2]. While respecting the interference threshold of a primary user (PU), a secondary user (SU) employing a spectrum underlay scheme is allowed to transmit on the licensed band of a PU [2]. Whereas, SUs deploying a spectrum overlay scheme transmit after locating *spectrum holes*, licensed to PUs, until a primary transmission is conducted on them [2], [3]. Being not in constant use in both the licensed and unlicensed bands, spectrum holes exist as temporary space–time–frequency voids [4]. The detection of these voids is known as spectrum sensing and hence the heart of communication systems that are based on CRs. Having attracted the attention of numerous researchers, a significant number of spectrum sensing techniques have been proposed over the years. Till recently, these techniques have been widely classified as *narrowband sensing* and *wideband sensing* techniques [5]–[7]. Upon the advent of *active sensing* techniques [8]–[10], a broader classification was reported recently. As per the very recent classification, spectrum sensing techniques can be classified as active sensing [8]–[10] and *quiet sensing* [2], [5]–[7], [11], [12].

To begin with, quiet sensing is performed by a SU which senses the channel for a fixed time-duration [8] and transmits afterward provided that the primary channel is idle. To overcome the capacity reduction due to quiet periods which are usually short to provide adequate samples for an accurate spectrum sensing [8], [9], and to surmount an extra burden of synchronization for the quiet periods [10] (for instance, the one needed in IEEE 802.22 intra-frame sensing [13]), active sensing has emerged as a promising spectrum sensing paradigm. In particular, the authors of [10] have proposed quiet-active sensing scheme by using inactive SUs which sense the channels in both quiet and active periods. At the cost of quiet-period synchronization [10], the advantage of this scheme over quiet sensing emanates from the additional samples obtained during the active period. To overcome the synchronization requirement of quiet-active sensing, the same authors have proposed an active sensing scheme—dubbed optimized active sensing—by placing quiet samples in the frequency domain so that selection diversity would be achieved [10]. On the contrary, the schemes of [10] require more spectrum resources and extra power resources are required because of the signaling overhead, and sensing of the primary signal and transmission of the sensing information to the active SU, respectively [8], [9].

Capitalizing on the three-port antenna based spatial filtering technique of [14], the authors of [9] have introduced a simultaneous sensing and data transmission technique by deploying a spatial isolation technique on the antennas of each cognitive node. Relying on the self-interference cancellation technique, the proposed scheme divides the spatial resources so that some antennas are devoted for spectrum sensing while others for data transmission [8]. Nevertheless, this very technique suffers from large self-interference produced during spectrum sensing and an appropriate physical distance should be maintained between the sensing and transmitting antennas [8]. To alleviate these issues, [8] is the latest advancement which has investigated a distributed multiple-input multiple-output (MIMO) CR-based system operating in the presence of multiple PUs. In particular, the paper proposes a communication protocol made of training, data transmission, and spectrum sensing phases which alternate periodically. After the introductory training

978-1-5386-6876-4/18/$31.00 ©2018 IEEE

phase, the paper assumes a spectrum sensing per every symbol duration prior to a transmission by the secondary nodes, and a joint minimum mean squared error detection and an energy detection based spectrum sensing. Hence, whenever a *hidden terminal* problem [7], [11] arises, the aforementioned protocol will keep on conducting a secondary transmission and emitting interference to a primary receiver which may not be blocked, unlike the blocked primary transmitter. To reliably detect a hidden primary terminal's signal exhibiting a very low signal-to-noise ratio (SNR), robust quiet spectrum sensing techniques are, thus, required. These techniques, as mentioned, can be either narrowband or wideband techniques.

As per the bandwidth of the signal to be detected, quiet spectrum sensing techniques can be *narrowband* or *wideband* [6], [15]–[17]. The wideband techniques can be Nyquist based or sub-Nyquist based depending on the adopted sampling rate [5], [16]. Sub-Nyquist sampling techniques usually deploy either compressive sampling [18] or multi-coset sampling [19]. On the other hand, Nyquist based wideband sensing techniques are based on either fast Fourier transforms [20], wavelets [21], or filter-banks [22]. Delving into narrowband sensing, several narrowband spectrum sensing techniques have been proposed over the years [2], [5], [6], [11]. The conventional ones are energy detection (ED) [23]–[25], matched filtering [26], feature-based detection [27], polarization detection [28], sample covariance matrix (SCM) based algorithms [29]–[32], moment ratio detection [33], and max-min detection [34], [35]. Nevertheless, ED relies on the known power spectral density of the noise and exhibits a high sensitivity to noise uncertainty [2], [11] leading to a poor performance at a low SNR regardless of the number of intercepted samples, as demonstrated via *SNR walls* [36]; matched filters suffer from intrinsic computational complexity and hence are unattractive for practical spectrum sensing applications; particular features need to be introduced to deploy feature detectors in OFDM-based communications [2]; polarization detectors are computationally complex and sensitive to estimation errors [28]; SCM-based techniques suffer from performance loss under sample-starved settings—despite their blindness—and their asymptotic threshold differs considerably from the exact value for finite sensors and samples, as attested by [29]; a moment ratio detection is computationally complex and relies on the asymptotic Gaussian distribution; and max-min detector suffer from huge computational complexity.

B. Motivation

Apart from the highlighted conventional algorithms, some other algorithms such as Bartlett estimate-based energy detection [37], a frequency domain eigenvalue-based spectrum sensing algorithms [38], subband energy-based spectrum sensing algorithm [39], energy detection spectrum sensing under RF imperfections and with multiple PUs [40], [41], and a robust estimator-correlator and a robust generalized likelihood detectors [42] have been proposed. However, all these important contributions are less attractive for practical CR applications since they rely on the complex Gaussian distributed primary signal. Recently, the F–test (FT) based spectrum sensing technique was proposed in [43] and corroborated to be superior over an energy detector, a maximum-minimum eigenvalue (MME) detector [30], and a generalized likelihood ratio test (GLRT) detector [44], [45], especially at low SNR. While exhibiting a moderate computational complexity, this detector is also robust against noise uncertainty and independent of noise power. However, it requires a prior knowledge of the channel state information (CSI) between the primary transmitter and secondary receiver rendering it susceptible to CSI estimation errors. Moreover, the FT detector of [43] assume a single-antenna primary transmitter which is not necessarily the case for the transmitters of the fourth generation (4G) and 5G era, as they are usually equipped with a massive number of antennas for the sake of array gain, spatial diversity gain, spatial multiplexing gain, and interference reduction [46]. Consequently, a robust and computationally simple spectrum sensing technique applicable to a MIMO CR network is crucial.

C. Contributions

Inspired by the FT detector of [43], [47] disseminates the modified versions of [43] which do not require the knowledge of CSI nor the noise power. These modified detectors were proposed for a single-input multiple-output (SIMO) CR network and a generalization to a MIMO CR network was also highlighted in [47]. Following the lead of [47], for a multi-antenna spectrum sensing over frequency selective channels, this paper presents—in detail—a detector named the MIMO CR generalized F–test via singular value decomposition (MIMO CR g-FT-v-SVD). This detector is applicable for the MIMO cognitive radio network and the contributions of this paper are itemized below.

- By deploying the estimation theory of a population covariance matrix (PCM) and different F–distributions, the exact and asymptotic performance analyses of the MIMO CR g-FT-v-SVD are presented.
- The performance of the MIMO CR g-FT-v-SVD is assessed through several Monte-Carlo simulations which also validate the derived analytical expressions.

Following this introduction, Sec. II presents the system model. Sec. III details the MIMO CR g-FT-v-SVD algorithm whose performance analyses are detailed in Sec. IV along with Appendices A and B. Sec. V reports the simulation results leading to paper conclusions drawn in Sec. VI.

Notation: Scalars, vectors, and matrices are denoted by italic letters, lower-case boldface letters, and upper-case boldface letters, respectively; $\sim$, $\propto$, $||\cdot||$, $\mathbb{C}^{N_R}$, and $\mathbb{H}^{N_R\times N_R}$ mean distributed as, statistically equivalent, the Euclidean norm, the sets of N_R–dimensional vectors of complex numbers, and of $N_R \times N_R$ Hermitian matrices, respectively; lim, $(\cdot)^T$, $(\cdot)^H$, $\mathbb{E}\{\cdot\}$, $\Pr\{\cdot\}$, and $\mathcal{CN}_{N_R}(\mathbf{0}, \mathbf{\Sigma})$ stand for limit, transpose, Hermitian, expectation, the probability of, and a zero mean circularly symmetric complex additive white Gaussian noise (AWGN) with a covariance matrix of $\mathbf{\Sigma} \in \mathbb{H}^{N_R\times N_R}$, respectively; $\mathrm{tr}(\cdot)$, $\mathrm{diag}(\cdot)$, $\boldsymbol{A}(:, j)$, $\boldsymbol{A}(:, i : j)$, and $\boldsymbol{I}_{N_R W}$ denote

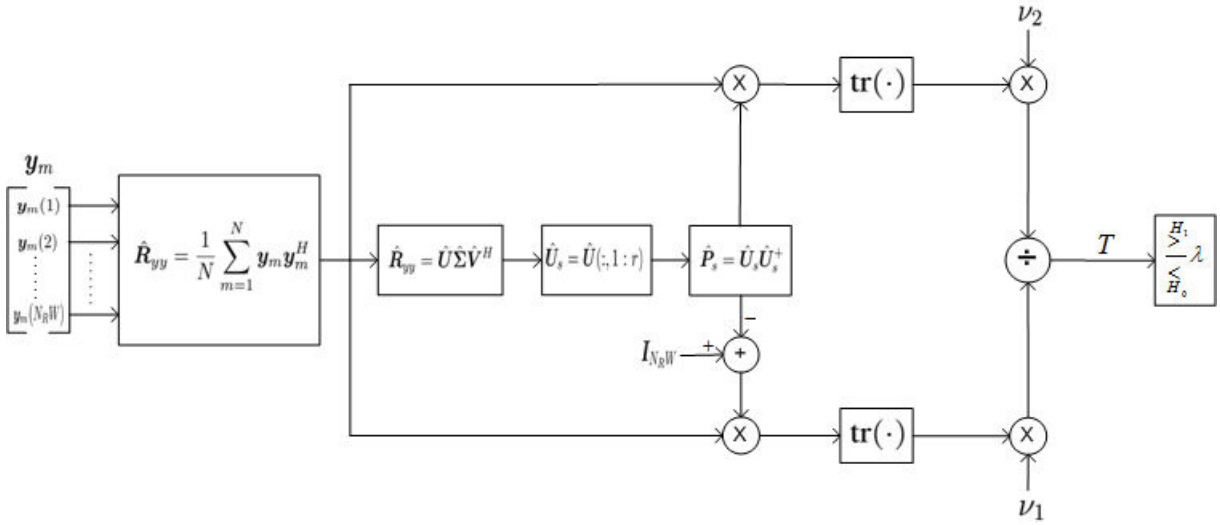

Fig. 1. The MIMO CR g-FT-v-SVD detector for $(\nu_1, \nu_2) = \big(2Nr, 2N(N_RW - r)\big)$ and $r = N_T(W + L)$.

trace, diagonal (block diagonal) matrix, the jth column of $\boldsymbol{A}$, the columns of $\boldsymbol{A}$ between its ith and jth columns including its ith and jth columns, and an $N_RW \times N_RW$ identity matrix, respectively; χ^2, F_{ν_1,ν_2}, $F'_{\nu_1,\nu_2}(\lambda_1)$, and $F''_{\nu_1,\nu_2}(\lambda_1,\lambda_2)$ denote the chi-square, the central F–distribution with (ν_1, ν_2) degrees of freedom (DoF), the singly non-central F–distribution with (ν_1, ν_2) DoF and non-centrality parameter (NCP) λ_1, and the doubly non-central F–distribution with (ν_1, ν_2) DoF and NCPs (λ_1, λ_2), respectively; and $F(\lambda; \nu_1, \nu_2)$, $F'(\lambda; \nu_1, \nu_2|\lambda_1)$, and $F''(\lambda; \nu_1, \nu_2|\lambda_1, \lambda_2)$ implicate the cumulative distribution function (CDF) of F_{ν_1,ν_2}, the CDF of $F'_{\nu_1,\nu_2}(\lambda_1)$, and the CDF of $F''_{\nu_1,\nu_2}(\lambda_1,\lambda_2)$, respectively, evaluated at λ.

II. System Model

Consider a MIMO CR network made of a primary transmitter with N_T antennas and a secondary receiver with N_R antennas. For an opportunistic transmission, the SU senses the licensed band of a PU through a frequency selective channel modeled as a finite-duration impulse response filter with $L+1$ taps. Toward this end, a binary hypothesis test is formulated on the presence or absence of a primary signal. Based on the system model in [48, Sec. II-A], the kth received and sampled baseband signal $\boldsymbol{y}[k] \in \mathbb{C}^{N_R}$ is expressed via a binary hypothesis test as

$$\boldsymbol{y}[k] = \begin{cases} \sum_{l=0}^{L} \boldsymbol{H}_l \boldsymbol{s}[k-l] + \boldsymbol{z}[k] & : H_1 \\ \boldsymbol{z}[k] & : H_0, \end{cases} \tag{1}$$

where H_0 and H_1 are, respectively, hypotheses regarding the idleness and activeness of a PU; $\boldsymbol{s}[k] = \big[s_1[k], s_2[k], \ldots, s_{N_T}[k]\big]^T \in \mathbb{C}^{N_T}$ denotes the kth symbol vector transmitted through N_T transmit antennas for $s_j[k]$ being the kth unknown and deterministic primary symbol emitted by the jth primary antenna; $\boldsymbol{H}_l \in \mathbb{C}^{N_R \times N_T}$ comprises the MIMO channel impulse responses corresponding to the lth multi-path fading component; and $\boldsymbol{z}[k] \sim \mathcal{CN}_{N_R}(\boldsymbol{0}, \boldsymbol{\Sigma})$. For σ^2 being the noise power, we assume *independent and identically distributed* (i.i.d.) noises such that $\boldsymbol{\Sigma} = \sigma^2 \boldsymbol{I}_{N_R}$.

III. The MIMO CR g-FT-v-SVD: Algorithm

A. The Formulated F–test

Stacking the observations of the secondary antennas into a highly structured vector with respect to (w.r.t.) the mth short term interval (STI) gives

$$\boldsymbol{y}_m = \begin{cases} \boldsymbol{H}\boldsymbol{s}_m + \boldsymbol{z}_m & : H_1 \\ \boldsymbol{z}_m & : H_0, \end{cases} \tag{2}$$

where $\boldsymbol{y}_m \in \mathbb{C}^{N_RW}$, $\boldsymbol{s}_m = \big[\boldsymbol{s}_{1m}^T, \boldsymbol{s}_{2m}^T, \ldots, \boldsymbol{s}_{N_Tm}^T\big]^T \in \mathbb{C}^{N_T(W+L)}$ for $\boldsymbol{s}_{jm} = \big[s_j[mW], s_j[mW-1], \ldots, s_j[mW - W - L + 1]\big]^T \in \mathbb{C}^{(W+L)}$ [48], and $\boldsymbol{H} \in \mathbb{C}^{N_RW \times N_T(W+L)}$ is the MIMO filtering matrix—made of banded Toeplitz matrices—as defined in [48, eqs. (3)-(5)], and $\boldsymbol{z}_m \sim \mathcal{CN}_{N_RW}(\boldsymbol{0}, \sigma^2 \boldsymbol{I}_{N_RW})$.

Employing (2), the corresponding SCM $\hat{\boldsymbol{R}}_{yy} \in \mathbb{C}^{N_RW \times N_RW}$ is computed as

$$\hat{\boldsymbol{R}}_{yy} = \frac{1}{N}\sum_{m=1}^{N} \boldsymbol{y}_m \boldsymbol{y}_m^H = \frac{1}{N}\boldsymbol{Y}\boldsymbol{Y}^H, \tag{3}$$

where N is the number of STIs and $\boldsymbol{Y} = [\boldsymbol{y}_1, \boldsymbol{y}_2, \ldots, \boldsymbol{y}_N]$. From (2), the PCM under H_1 becomes [48, eq. (6)]

$$\boldsymbol{R}_{yy} = \mathbb{E}\{\boldsymbol{y}_m \boldsymbol{y}_m^H\} = \boldsymbol{H}\boldsymbol{R}_{ss}\boldsymbol{H}^H + \sigma^2 \boldsymbol{I}_{N_RW}, \tag{4}$$

where $\boldsymbol{R}_{ss} = \mathbb{E}\{\boldsymbol{s}_m \boldsymbol{s}_m^H\} \in \mathbb{C}^{r \times r}$—$r = N_T(W+L)$—denotes the primary data correlation matrix which indicates an $N_RW \times r$ dimensional primary signal subspace. Applying SVD to (3),

$$\hat{\boldsymbol{R}}_{yy} = \hat{\boldsymbol{U}}\hat{\boldsymbol{\Sigma}}\hat{\boldsymbol{V}}^H = [\hat{\boldsymbol{U}}_s\ \hat{\boldsymbol{U}}_n]\hat{\boldsymbol{\Sigma}}\hat{\boldsymbol{V}}^H, \tag{5}$$

where $\hat{\boldsymbol{U}}_s = \hat{\boldsymbol{U}}(:, 1:r) \in \mathbb{C}^{N_RW \times r}$ denotes the estimated subspace spanned by the eigenvectors corresponding to the largest r eigenvalues, $\hat{\boldsymbol{U}}_n = \hat{\boldsymbol{U}}(:, r+1:$

$N_R W) \in \mathbb{C}^{N_R W \times (N_R W - r)}$ represents the estimated subspace spanned by the eigenvectors corresponding to the remaining $N_R W - r$ eigenvalues, and $\hat{\boldsymbol{\Sigma}} = \text{diag}\big(\hat{\boldsymbol{\Sigma}}_s, \hat{\boldsymbol{\Sigma}}_n\big)$ for $\hat{\boldsymbol{\Sigma}}_s = \text{diag}\big(\hat{\sigma}_1, \hat{\sigma}_2, \ldots, \hat{\sigma}_r\big)$, $\hat{\boldsymbol{\Sigma}}_n = \text{diag}\big(\hat{\sigma}_{r+1}, \hat{\sigma}_{r+2}, \ldots, \hat{\sigma}_{N_R W}\big)$, and $\hat{\sigma}_i$ being the ith singular value. To identify the primary signal subspace under H_1, meanwhile, we make these assumptions similar to [48]: $N_T < N_R$, $N \geq N_T(W + L)$, $N_R W \geq N_T(W + L)$, and $W > L$.

Deploying (3) and a projection matrix $\hat{\boldsymbol{P}}_s \in \mathbb{C}^{N_R W \times N_R W}$ defined as $\hat{\boldsymbol{P}}_s = \hat{\boldsymbol{U}}_s \hat{\boldsymbol{U}}_s^H$, the MIMO CR g-FT-v-SVD test statistic and decision rule are formulated as

$$T \triangleq \frac{\nu_2}{\nu_1} \frac{\text{tr}(\hat{\boldsymbol{P}}_s \hat{\boldsymbol{R}}_{yy})}{\text{tr}\big((\boldsymbol{I}_{N_R W} - \hat{\boldsymbol{P}}_s)\hat{\boldsymbol{R}}_{yy}\big)} \underset{H_0}{\overset{H_1}{\gtrless}} \lambda, \tag{6}$$

where $(\nu_1, \nu_2) = \big(2Nr, 2N(N_R W - r)\big)$ are the DoF and λ is the decision threshold. Meanwhile, the MIMO CR g-FT-v-SVD detector is depicted in Fig. 1.

Remark 1: Unlike [43, eq. (5)], (6) is independent of the knowledge of the CSI between the primary transmitter and the secondary receiver.

B. Equivalent Test Statistic

To derive the equivalent MIMO CR g-FT-v-SVD test statistic, we first note that the SCM is a Hermitian as well as a positive semi-definite matrix. Hence, its eigenvalue decomposition and SVD are identical and hence $\hat{\boldsymbol{U}} = \big[\hat{\boldsymbol{U}}_s, \hat{\boldsymbol{U}}_n\big] = \hat{\boldsymbol{V}} = \big[\hat{\boldsymbol{V}}_s, \hat{\boldsymbol{V}}_n\big]$. To continue, substituting $\hat{\boldsymbol{P}}_s = \hat{\boldsymbol{U}}_s \hat{\boldsymbol{U}}_s^H$ and (5) into (6) gives

$$T = \frac{N_R W - r}{r} \frac{\text{tr}(\hat{\boldsymbol{U}}_s \hat{\boldsymbol{\Sigma}}_s \hat{\boldsymbol{U}}_s^H)}{\text{tr}\big(\hat{\boldsymbol{U}}_n \hat{\boldsymbol{\Sigma}}_n \hat{\boldsymbol{U}}_n^H\big)} \tag{7a}$$

$$\overset{(a)}{=} \frac{N_R W - r}{r} \frac{\text{tr}(\hat{\boldsymbol{U}}_s^H \hat{\boldsymbol{U}}_s \hat{\boldsymbol{\Sigma}}_s)}{\text{tr}\big(\hat{\boldsymbol{U}}_n^H \hat{\boldsymbol{U}}_n \hat{\boldsymbol{\Sigma}}_n\big)} \tag{7b}$$

$$\overset{(b)}{=} \frac{N_R W - r}{r} \frac{\text{tr}(\hat{\boldsymbol{\Sigma}}_s)}{\text{tr}\big(\hat{\boldsymbol{\Sigma}}_n\big)} = \frac{N_R W - r}{r} \frac{\sum_{i=1}^{r} \hat{\sigma}_i}{\sum_{i=r+1}^{N_R W} \hat{\sigma}_i}, \tag{7c}$$

where (a) follows for $\text{tr}(\boldsymbol{AB}) = \text{tr}(\boldsymbol{BA})$ [49] and (b) is true for $\hat{\boldsymbol{U}} = [\hat{\boldsymbol{U}}_s \; \hat{\boldsymbol{U}}_n]$ is an orthonormal matrix. Hence, it can be inferred from (7c) that

$$T \propto \frac{\sum_{i=1}^{r} \hat{\sigma}_i}{\sum_{i=r+1}^{N_R W} \hat{\sigma}_i}. \tag{8}$$

Remark 2: To reduce the computational complexity of the MIMO CR g-FT-v-SVD detector, it can be implemented via (8) as an eigenvalue detector.

IV. Performance Analyses

Realizing that (6), respectively, admits a doubly non-central F–distribution and a central F–distribution under H_1 and H_0, the underneath exact analysis follows. By employing the estimation theory of a PCM, an asymptotic performance analysis of the MIMO CR g-FT-v-SVD also follows.

A. Exact Analysis

Substituting (2) into (3) and, in turn, into (6),

$$T|H_1 = \frac{\nu_2}{\nu_1} \frac{F_1|H_1}{F_2|H_1}, \tag{9}$$

where $F_1|H_1 = \sum_{m=1}^{N} \big(\boldsymbol{H}\boldsymbol{s}_m + \boldsymbol{z}_m\big)^H \hat{\boldsymbol{P}}_s \big(\boldsymbol{H}\boldsymbol{s}_m + \boldsymbol{z}_m\big)$ and $F_2|H_1 = \sum_{m=1}^{N} \big(\boldsymbol{H}\boldsymbol{s}_m + \boldsymbol{z}_m\big)^H \big(\boldsymbol{I}_{N_R W} - \hat{\boldsymbol{P}}_s\big) \big(\boldsymbol{H}\boldsymbol{s}_m + \boldsymbol{z}_m\big)$. As $T|H_1$ is the ratio of two non-central χ^2–distributed random variables (RVs), $T|H_1 \sim F''_{\nu_1,\nu_2}(\lambda_1^{H_1}, \lambda_2^{H_1})$ [43], where $\big(\lambda_1^{H_1}, \lambda_2^{H_1}\big) = \frac{2}{\sigma^2} \sum_{m=1}^{N} \big(\big|\big|\hat{\boldsymbol{P}}_s \boldsymbol{H}\boldsymbol{s}_m\big|\big|^2, \big|\big|\big(\boldsymbol{I}_{N_R W} - \hat{\boldsymbol{P}}_s\big)\boldsymbol{H}\boldsymbol{s}_m\big|\big|^2\big)$.

Similarly, the test statistic under H_0 becomes

$$T|H_0 = \frac{\nu_2}{\nu_1} \frac{F_1|H_0}{F_2|H_0}, \tag{10}$$

where $F_1|H_0 = \sum_{k=1}^{N} \boldsymbol{z}_m^H \hat{\boldsymbol{P}}_s \boldsymbol{z}_m$ and $F_2|H_0 = \sum_{m=1}^{N} \boldsymbol{z}_m^H (\boldsymbol{I}_{N_R W} - \hat{\boldsymbol{P}}_s) \boldsymbol{z}_m$. The right-hand side of (10) is a ratio of two central χ^2–distributed RVs. Thus, $T|H_0 \sim F_{\nu_1,\nu_2}$ [43]. The exact $P_f = \Pr\{T|H_0 > \lambda\}$ exhibited by the MIMO CR g-FT-v-SVD becomes

$$P_f = 1 - \Pr\big\{T|H_0 \leq \lambda\big\} = 1 - F\big(\lambda; \nu_1, \nu_2\big). \tag{11}$$

Similarly, the exact P_d for a given λ is computed as

$$P_d = \Pr\big\{T|H_1 > \lambda\big\} = 1 - \Pr\big\{T|H_1 \leq \lambda\big\}. \tag{12}$$

Since $T|H_1 \sim F''_{\nu_1,\nu_2}(\lambda_1^{H_1}, \lambda_2^{H_1})$, (12) simplifies to

$$P_d = 1 - F''\big(\lambda; \nu_1, \nu_2 \big| \lambda_1^{H_1}, \lambda_2^{H_1}\big). \tag{13}$$

B. Asymptotic Analysis

For infinitely large samples, the estimation theory of a PCM corroborates that the SCM perfectly approximates the PCM. Accordingly, the asymptotic P_d w.r.t. N is characterized via the following theorem.

Theorem 1:

$$\lim_{N \to \infty} P_d = 1 - F'(\lambda; \nu_1, \nu_2 | \lambda^{H_1}), \tag{14}$$

where $\lambda^{H_1} = \lim_{N \to \infty} \frac{2}{\sigma^2} \sum_{m=1}^{N} \big|\big|\boldsymbol{H}\boldsymbol{s}_m\big|\big|^2$. For $\bar{\gamma}_{snr}^{\infty} = \lim_{N \to \infty} \frac{1}{N} \sum_{m=1}^{N} \frac{\big|\big|\boldsymbol{H}\boldsymbol{s}_m\big|\big|^2}{N_R W \sigma^2}$ being the average SNR over an infinite duration, $\lim_{N \to \infty} P_d = 0$ provided that $\lambda > \frac{N_R W - r}{r} \bar{\gamma}_{snr}^{\infty}$.

Proof: Please refer to Appendix A.

Similarly, the PCM estimation theory is deployed to characterize the exhibited asymptotic P_f which is stated beneath.

Corollary 1: Whenever $\lambda > 0$,

$$\lim_{N \to \infty} P_f = 0. \tag{15}$$

Proof: Please see Appendix B.

Remark 3: As $N \to \infty$, the MIMO CR g-FT-v-SVD exhibits a null probability of false alarm.

Simulation parameters	Assigned value
(W, L)	$(3, 1)$
(P_s, N)	$(10\ \text{W}, 100)$
No. of realizations	10^4

TABLE I
SIMULATION PARAMETERS UNLESS OTHERWISE MENTIONED.

V. SIMULATION RESULTS

Unless otherwise mentioned, this section provides Monte-Carlo simulations and/or analytical performance assessments of the MIMO CR g-FT-v-SVD by using the simulation parameters of Table I. We consider a quadrature phase shift keying (QPSK) modulated primary signal, i.e, $s_j[k] = \sqrt{P_s/2}\big[s_{kj}^I + js_{kj}^Q\big]$ for P_s being the transmitted—through the jth transmit antenna—primary power, $\{s_k^I, s_k^Q\} \in \{-1, 1\} \times \{-1, 1\}$, and $1 \leq j \leq N_T$. Without loss of generality and similar to [50], we assume that the elements of $\boldsymbol{H}_l$ exhibit the Gaussian distribution with zero mean and unit variance, i.e., $\boldsymbol{H}_l(i, j) \sim \mathcal{CN}_1(0, 1)$, $0 \leq l \leq L$, $1 \leq i \leq N_R$, and $1 \leq j \leq N_T$. For the target false alarm rate (FAR) of 0.1, the corresponding MIMO CR g-FT-v-SVD decision threshold λ is obtained via the implementation—under H_0—of the test statistic in (6) followed by averaging over 10^6 realizations. The MIMO CR g-FT-v-SVD is simulated via the test statistic in (6) for an SNR defined as $\gamma_{snr} = \big|\big|\boldsymbol{H}\boldsymbol{s}_m\big|\big|^2/N_R W\sigma^2$. Moreover, the false alarm plots are simulated by considering the samples of an AWGN of power σ^2 as an input. Hereinafter, the performance comparison with the state-of-the-art, validation of the closed-form expressions, and the FAR and complementary receiver operating characteristics (ROC) curves are reported.

A. Performance Comparison with the State-of-the-Art

As almost all the state-of-the-art multi-antenna detectors consider a PU equipped with a single antenna, we, first, compare the performance of the MIMO CR g-FT-v-SVD detector which assumes single transmitting antenna with the state-of-the-art detectors. In this respect, Fig. 2 showcases the detection performance of the state-of-the-art detectors with the MIMO CR g-FT-v-SVD's.

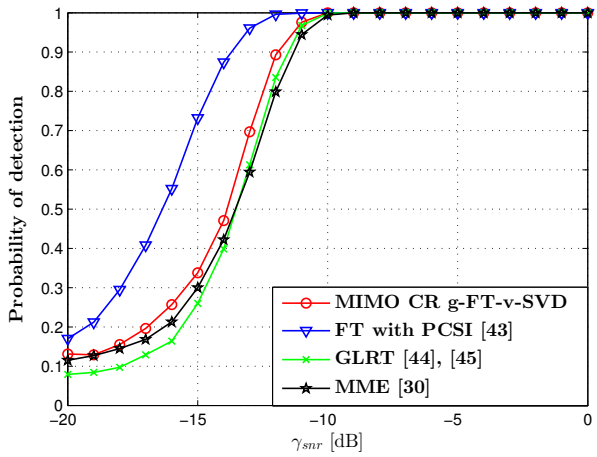

Fig. 2. P_d versus γ_{snr}: $(N_R, N_T) = (5, 1)$, $N = 300$, and $P_f = 0.1$.

For the detection of a primary signal manifesting a very low SNR, Fig. 2 showcases that the MIMO CR g-FT-v-SVD improves both MME [30] and GLRT [44], [45]. The performance improvement is attributed to the fact that the performance of the MIMO CR g-FT-v-SVD depends on the quality of the primary signal subspace estimates. Moreover, it is corroborated by the same plot that the MIMO CR g-FT-v-SVD—with no CSI—performs as good as FT [43] fed with a perfect CSI (PCSI) for $\gamma_{snr} \geq -10$ dB. Such a performance at low SNR regimes can alleviate the *hidden terminal problem* [11] and serves the required SNR sensitivities for primary signals defined by the IEEE 802.22 working group [51].

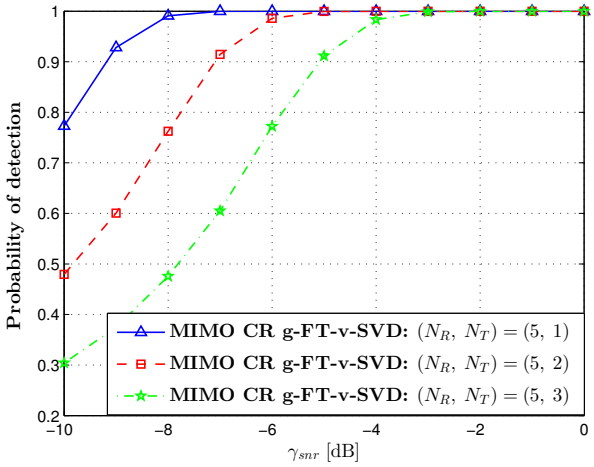

Fig. 3. P_d versus γ_{snr}: $P_f = 0.1$.

W.r.t. the desired FAR of 0.1, Figs. 3 depicts the detection performance of the MIMO CR g-FT-v-SVD. Specifically, it showcases the detection performance of the MIMO CR g-FT-v-SVD for different values of N_T. As it is seen, the P_d exhibited by the MIMO CR g-FT-v-SVD decreases with the increment of N_T. Such a performance loss is attributed to the fact that a large N_T results in a large primary signal subspace—estimated via (5)—which is naturally estimated poorly. In other words, the observed performance loss can also be explained via an increase in interference emitted by the neighboring transmitting antennas whenever N_T increases. Furthermore, Fig. 3 demonstrates that the MIMO CR g-FT-v-SVD exhibits an attractive detection performance—regardless of N_T—for the low SNR regimes which are usually a bottle-neck regarding the capacity of CR networks.

B. Validation of the Analytical Expressions

In order to validate the exact detection expression given by (13), Fig. 4 depicts the P_d versus λ curves for $\gamma_{snr} \in \{-5, 0\}$ dB. Here, it is to be noted that the approximations in [43, eqs. (21) and (22)] were deployed to depict the numerical results of (13). To continue, as observed in Fig. 4, the Monte-Carlo simulation results and the numerical results of (13) are in an overlap. Hence, the Monte-Carlo simulations validate (13). Moreover, the derived exact detection and FAR expressions—given by (11) and (13)—of the MIMO CR g-FT-v-SVD are

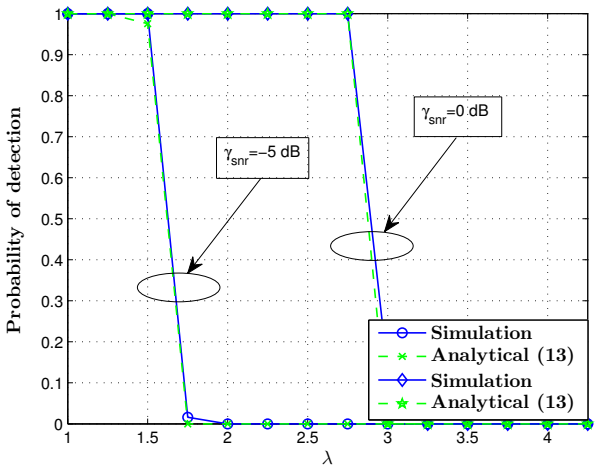

Fig. 4. P_d versus λ: $(N_R, N_T) = (5, 2)$.

validated further via the complementary ROC (CROC) curve depicted in Fig. 6.

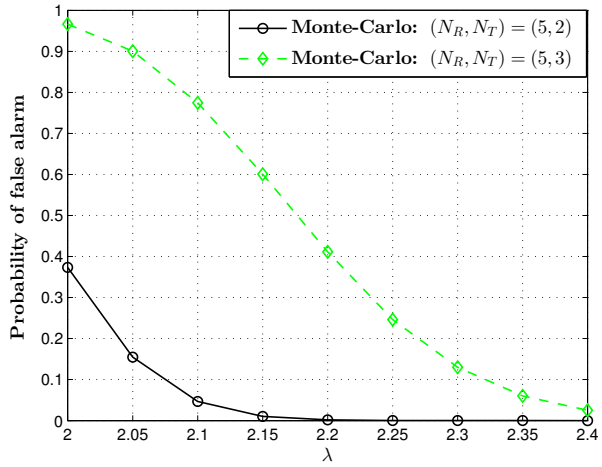

Fig. 5. P_f versus λ: 10^6 realizations.

C. The FAR and Complementary ROC Curves

To showcase the FAR and CROC exhibited by the MIMO CR g-FT-v-SVD, Figs. 5 and 6 depict the FAR and the CROC curves, respectively. To continue, Fig. 5 corroborates the P_f versus λ curves—exhibited by the MIMO CR g-FT-v-SVD—depicted for different (N_R, N_T) values. As seen, the exhibited FAR falls w.r.t. λ and increases w.r.t. N_T. The former and latter observations are, respectively, attributed to the fact that a larger threshold renders a smaller ambiguity on the absence of the primary signal and a larger N_T results in a larger primary subspace which is estimated—as discussed before—poorly.

The CROC manifested by the MIMO CR-g-FT-v-SVD is depicted via Fig. 6. It, specifically, demonstrates the probability of miss (P_m)—simulated as $P_m = 1 - P_d$—versus P_f characteristics exhibited by the MIMO CR-g-FT-v-SVD. As it is evident from Fig. 6, the exhibited P_m decreases with the increment of P_f and vice versa. Therefore, such a natural trade-off is corroborated via Fig. 6 which also validates (11) and (13).

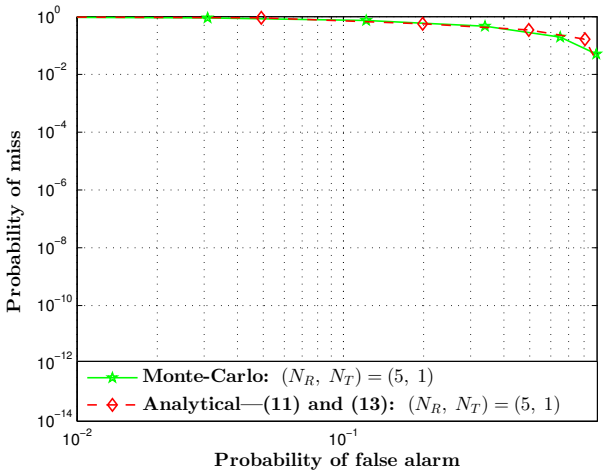

Fig. 6. The manifested CROC: $\gamma_{snr} = -15$ dB.

VI. Conclusions

In order to overcome the discrepancy between spectrum underutilization and spectrum scarcity, CR has emerged as a promising technology. For the operation of such a radio which employs an opportunistic spectrum access scheme, a robust and computationally simple spectrum sensing is the heart of its operation. In order to render a robust sensing, the underlying technique shall not rely on the knowledge of the noise power, the primary signal characteristics, or any type of CSI. Accordingly, a simple F–test based spectrum sensing technique named the MIMO CR g-FT-v-SVD—applicable for MIMO CR networks—is presented in detail. To elucidate the performance of the MIMO CR g-FT-v-SVD, exact and asymptotic closed-form expressions are derived. At last, the derived closed-form expressions are validated by the Monte-Carlo simulations which also corroborate the performance of the MIMO CR g-FT-v-SVD.

Appendix A
Proof of Theorem 1

As $N \to \infty$, the PCM under H_1 and its SVD are, respectively, given by $\boldsymbol{R}_{yy} = \mathbb{E}\{\boldsymbol{H}\boldsymbol{s}_m\boldsymbol{s}_m^H\boldsymbol{H}^H\} + \sigma^2\boldsymbol{I}_{N_RW}$ and

$$\boldsymbol{R}_{yy} = \boldsymbol{U}\boldsymbol{\Sigma}\boldsymbol{V}^H = [\boldsymbol{U}_s\ \boldsymbol{U}_n]\boldsymbol{\Sigma}[\boldsymbol{V}_s\ \boldsymbol{V}_n]^H, \tag{16}$$

where $\boldsymbol{U}_s = \boldsymbol{U}(:, 1:r)$ is the true primary signal subspace, $\boldsymbol{U}_n = \boldsymbol{U}(:, r+1 : N_RW)$ is the true noise subspace, and $\boldsymbol{\Sigma} = \text{diag}\big(\boldsymbol{\Sigma}_s, \boldsymbol{\Sigma}_n\big)$ for $\boldsymbol{\Sigma}_s = \text{diag}\big(\sigma_1, \sigma_1, \ldots, \sigma_r\big)$, $\boldsymbol{\Sigma}_n = \text{diag}\big(\sigma_{r+1}, \sigma_{r+2}, \ldots, \sigma_{N_RW}\big)$, and $\sigma_1 \geq \sigma_2 \geq \ldots \geq \sigma_{N_RW}$. As $N \to \infty$, the SOI and noise subspaces are perfectly estimated. Hence, we can infer that

$$\mathbb{E}\{\boldsymbol{H}\boldsymbol{s}_m\boldsymbol{s}_m^H\boldsymbol{H}^H\} = \boldsymbol{U}_s\boldsymbol{\Sigma}_s\boldsymbol{V}_s^H \tag{17a}$$

$$\sigma^2\boldsymbol{I}_{N_RW} = \boldsymbol{U}_n\boldsymbol{\Sigma}_n\boldsymbol{V}_n^H. \tag{17b}$$

As $N \to \infty$, the SCM perfectly estimates the PCM, i.e., $\lim_{N\to\infty} \hat{\boldsymbol{R}}_{yy} = \boldsymbol{R}_{yy}$. Hence,

$$\lim_{N\to\infty} \hat{\boldsymbol{P}}_s = \boldsymbol{P}_s = \boldsymbol{U}_s \boldsymbol{U}_s^H. \tag{18}$$

From the decision rule,

$$\lim_{N\to\infty} P_d = \lim_{N\to\infty} \Pr\{T|H_1 > \lambda\} \tag{19a}$$

$$= \Pr\{ \lim_{N\to\infty} T|H_1 > \lambda\}. \tag{19b}$$

Utilizing (6) and applying the properties of limit,

$$\lim_{N\to\infty} T|H_1 = \frac{\nu_2}{\nu_1} \frac{\mathrm{tr}\big(\lim_{N\to\infty} \hat{\boldsymbol{P}}_s \lim_{N\to\infty} \hat{\boldsymbol{R}}_{yy}\big)}{\mathrm{tr}\big((\boldsymbol{I}_{N_R W} - \lim_{N\to\infty} \hat{\boldsymbol{P}}_s) \lim_{N\to\infty} \hat{\boldsymbol{R}}_{yy}\big)} \tag{20a}$$

$$= \frac{\nu_2}{\nu_1} \frac{\mathrm{tr}\big(\boldsymbol{P}_s \boldsymbol{R}_{yy}\big)}{\mathrm{tr}\big((\boldsymbol{I}_{N_R W} - \boldsymbol{P}_s)\boldsymbol{R}_{yy}\big)}. \tag{20b}$$

Expressing $\boldsymbol{R}_{yy}$ via infinite summation of products,

$$\lim_{N\to\infty} T|H_1 = \lim_{N\to\infty} \frac{\nu_2}{\nu_1} \frac{\sum_{m=1}^{N} \tilde{\boldsymbol{y}}_m^H \boldsymbol{P}_s \tilde{\boldsymbol{y}}_m}{\sum_{m=1}^{N} \tilde{\boldsymbol{y}}_m^H \big(\boldsymbol{I}_{N_R W} - \boldsymbol{P}_s\big)\tilde{\boldsymbol{y}}_m}, \tag{21}$$

where $\tilde{\boldsymbol{y}}_m = \boldsymbol{H}\boldsymbol{s}_m + \boldsymbol{z}_m$.

Meanwhile, $\boldsymbol{P}_s$ and $\big(\boldsymbol{I}_{N_R W} - \boldsymbol{P}_s\big)$ perfectly project toward the primary signal and noise subspaces, respectively. Accordingly, $\lim_{N\to\infty} T|H_1 \sim F'_{\nu_1,\nu_2}(\lambda^{H_1})$ for λ^{H_1} being the NCP defined as

$$\lambda^{H_1} = \lim_{N\to\infty} \frac{2}{\sigma^2} \sum_{m=1}^{N} \Big(\big|\big|\boldsymbol{P}_s \boldsymbol{H}\boldsymbol{s}_m\big|\big|^2 = \big|\big|\boldsymbol{H}\boldsymbol{s}_m\big|\big|^2 \Big). \tag{22}$$

Thus,

$$\lim_{N\to\infty} P_d = \Pr\{ \lim_{N\to\infty} T|H_1 > \lambda\} \tag{23a}$$

$$= 1 - \Pr\{ \lim_{N\to\infty} T|H_1 \le \lambda\} \tag{23b}$$

$$= 1 - F'(\lambda; \nu_1, \nu_2 | \lambda^{H_1}). \tag{23c}$$

To further characterize the asymptotic P_d, we simplify (21). Substituting (16) and (18) into (20b) results in

$$\lim_{N\to\infty} T|H_1 = \frac{\nu_2 \mathrm{tr}\big(\boldsymbol{U}_s \boldsymbol{U}_s^H [\boldsymbol{U}_s\ \boldsymbol{U}_n] \boldsymbol{\Sigma} \boldsymbol{V}^H\big)}{\nu_1 \mathrm{tr}\big((\boldsymbol{I}_{N_R W} - \boldsymbol{U}_s \boldsymbol{U}_s^H)[\boldsymbol{U}_s\ \boldsymbol{U}_n] \boldsymbol{\Sigma} \boldsymbol{V}^H\big)}. \tag{24}$$

Recalling that $\boldsymbol{U}_s \boldsymbol{U}_s^H \boldsymbol{U}_s = \boldsymbol{U}_s$ and $\boldsymbol{U}_s^H \boldsymbol{U}_n = \boldsymbol{0}_{r\times(N_R W - r)}$, (24) simplifies to

$$\lim_{N\to\infty} T|H_1 = \frac{\nu_2}{\nu_1} \frac{\mathrm{tr}([\boldsymbol{U}_s\ \ \boldsymbol{0}_{N_R W \times (N_R W - r)}] \boldsymbol{\Sigma} \boldsymbol{V}^H)}{\mathrm{tr}\big([\boldsymbol{0}_{N_R W \times r}\ \ \boldsymbol{U}_n] \boldsymbol{\Sigma} \boldsymbol{V}^H\big)} \tag{25a}$$

$$= \frac{\nu_2}{\nu_1} \frac{\mathrm{tr}\big(\boldsymbol{U}_s \boldsymbol{\Sigma}_s \boldsymbol{V}_s^H\big)}{\mathrm{tr}\big(\boldsymbol{U}_n \boldsymbol{\Sigma}_n \boldsymbol{V}_n^H\big)} \tag{25b}$$

$$\overset{(b)}{=} \frac{\nu_2}{\nu_1} \frac{\mathbb{E}\big\{\mathrm{tr}\big(\boldsymbol{H}\boldsymbol{s}_m \boldsymbol{s}_m^H \boldsymbol{H}^H\big)\big\}}{\mathrm{tr}\big(\sigma^2 \boldsymbol{I}_{N_R W}\big)}, \tag{25c}$$

where (b) follows from (17a) and (17b).

Expressing expectation via the average of infinite summation of products gives

$$\lim_{N\to\infty} T|H_1 = \frac{N_R W - r}{r} \bar{\gamma}_{snr}^{\infty}, \tag{26}$$

where $\bar{\gamma}_{snr}^{\infty} = \lim_{N\to\infty} \frac{1}{N} \sum_{m=1}^{N} \frac{\big|\big|\boldsymbol{H}\boldsymbol{s}_m\big|\big|^2}{N_R W \sigma^2}$ is the average SNR defined over an infinite duration. Hence,

$$\lim_{N\to\infty} P_d = \Pr\{ \lim_{N\to\infty} T|H_1 > \lambda\} = \Pr\left\{ \frac{N_R W - r}{r} \bar{\gamma}_{snr}^{\infty} > \lambda \right\}. \tag{27}$$

Therefore, whenever $\lambda > \frac{N_R W - r}{r} \bar{\gamma}_{snr}^{\infty}$, $\lim_{N\to\infty} P_d = 0$. ■

Appendix B
Proof of Corollary 1

By definition,

$$\lim_{N\to\infty} P_f = \lim_{N\to\infty} \Pr\{T|H_0 > \lambda\} \tag{28a}$$

$$= \Pr\{ \lim_{N\to\infty} T|H_0 > \lambda\} = 1 - \Pr\{ \lim_{N\to\infty} T|H_0 \le \lambda\}. \tag{28b}$$

From (2), $T|H_0 = T|H_1\big|_{\{\boldsymbol{s}_m\}_{m=1}^{N}=0}$. Thus,

$$\lim_{N\to\infty} T|H_0 = \lim_{N\to\infty} T|H_1\big|_{\{\boldsymbol{s}_m\}_{m=1}^{N}=0}. \tag{29}$$

Using (21) in (29) results in

$$\lim_{N\to\infty} T|H_0 = \lim_{N\to\infty} \frac{\nu_2}{\nu_1} \frac{F_1|H_0}{F_2|H_0}, \tag{30}$$

where $F_1|H_0 = \sum_{m=1}^{N} \boldsymbol{z}_m^H \boldsymbol{P}_s \boldsymbol{z}_m$ and $F_2|H_0 = \sum_{m=1}^{N} \boldsymbol{z}_m^H (\boldsymbol{I}_{N_R W} - \boldsymbol{P}_s)\boldsymbol{z}_m$. Accordingly, $\lim_{N\to\infty} T|H_0 \sim F_{\nu_1,\nu_2}$ and hence

$$\lim_{N\to\infty} P_f = 1 - F(\lambda; \nu_1, \nu_2). \tag{31}$$

To characterize P_f further, we deploy (26) in (29). Doing so results in

$$\lim_{N\to\infty} T|H_0 = 0. \tag{32}$$

Using (32) in (28a), $\lim_{N\to\infty} P_f = \Pr\{ \lim_{N\to\infty} T|H_0 > \lambda\} = \Pr\{0 > \lambda\}$. If $\lambda > 0$, thus, $\lim_{N\to\infty} P_f = 0$. ■

Acknowledgment

The authors acknowledge the funding provided by AVIO-601 Project.

References

[1] Q. Zhao and B. M. Sadler, "A survey of dynamic spectrum access," *IEEE Signal Process. Mag.*, vol. 24, no. 3, pp. 79–89, May 2007.

[2] B. Wang and K. J. R. Liu, "Advances in cognitive radio networks: A survey," *IEEE J. Sel. Topics Signal Process.*, vol. 5, no. 1, pp. 5–23, Feb. 2011.

[3] S. Haykin, "Cognitive radio: brain-empowered wireless communications," *IEEE J. Sel. Areas Commun.*, vol. 23, no. 2, pp. 201–220, Feb. 2005.

[4] A. Goldsmith, S. A. Jafar, I. Maric, and S. Srinivasa, "Breaking spectrum gridlock with cognitive radios: An information theoretic perspective," *Proc. IEEE*, vol. 97, no. 5, pp. 894–914, May 2009.

[5] A. Ali and W. Hamouda, "Advances on spectrum sensing for cognitive radio networks: Theory and applications," *IEEE Commun. Surveys Tuts.*, vol. 19, no. 2, pp. 1277–1304, 2nd Quart., 2017.

[6] S. K. Sharma, T. E. Bogale, S. Chatzinotas, B. Ottersten, L. B. Le, and X. Wang, "Cognitive radio techniques under practical imperfections: A survey," *IEEE Commun. Surveys Tuts.*, vol. 17, no. 4, pp. 1858–1884, 4th Quart., 2015.

[7] T. Yucek and H. Arslan, "A survey of spectrum sensing algorithms for cognitive radio applications," *IEEE Commun. Surveys Tuts.*, vol. 11, no. 1, pp. 116–130, 1st Quart., 2009.

[8] N. I. Miridakis, T. A. Tsiftsis, G. C. Alexandropoulos, and M. Debbah, "Simultaneous spectrum sensing and data reception for cognitive spatial multiplexing distributed systems," *IEEE Trans. Wireless Commun.*, vol. 16, no. 5, pp. 3313–3327, May 2017.

[9] J. Heo, H. Ju, S. Park, E. Kim, and D. Hong, "Simultaneous sensing and transmission in cognitive radio," *IEEE Trans. Wireless Commun.*, vol. 13, no. 4, pp. 1948–1959, Apr. 2014.

[10] S. H. Song, K. Hamdi, and K. B. Letaief, "Spectrum sensing with active cognitive systems," *IEEE Trans. Wireless Commun.*, vol. 9, no. 6, pp. 1849–1854, Jun. 2010.

[11] E. Axell, G. Leus, E. G. Larsson, and H. V. Poor, "Spectrum sensing for cognitive radio : State-of-the-art and recent advances," *IEEE Signal Process. Mag.*, vol. 29, no. 3, pp. 101–116, May 2012.

[12] S. Haykin, D. J. Thomson, and J. H. Reed, "Spectrum sensing for cognitive radio," *Proc. IEEE*, vol. 97, no. 5, pp. 849–877, May 2009.

[13] C. R. Stevenson, G. Chouinard, Z. Lei, W. Hu, S. J. Shellhammer, and W. Caldwell, "IEEE 802.22: The first cognitive radio wireless regional area network standard," *IEEE Commun. Mag.*, vol. 47, no. 1, pp. 130–138, Jan. 2009.

[14] E. Tsakalaki, O. N. Alrabadi, A. Tatomirescu, E. de Carvalho, and G. F. Pedersen, "Concurrent communication and sensing in cognitive radio devices: Challenges and an enabling solution," *IEEE Trans. Antennas Propag.*, vol. 62, no. 3, pp. 1125–1137, Mar. 2014.

[15] T. E. Bogale, L. Vandendorpe, and L. B. Le, "Wide-band sensing and optimization for cognitive radio networks with noise variance uncertainty," *IEEE Trans. Commun.*, vol. 63, no. 4, pp. 1091–1105, Apr. 2015.

[16] H. Sun, A. Nallanathan, C. X. Wang, and Y. Chen, "Wideband spectrum sensing for cognitive radio networks: A survey," *IEEE Wireless Commun.*, vol. 20, no. 2, pp. 74–81, Apr. 2013.

[17] S. K. Jayaweera, *Signal Processing for Cognitive Radios*, 1st ed. Hoboken, NJ, USA: Wiley, 2014.

[18] D. L. Donoho, "Compressed sensing," *IEEE Trans. Inf. Theory*, vol. 52, no. 4, pp. 1289–1306, Apr. 2006.

[19] R. Venkataramani and Y. Bresler, "Perfect reconstruction formulas and bounds on aliasing error in sub-Nyquist nonuniform sampling of multiband signals," *IEEE Trans. Inf. Theory*, vol. 46, no. 6, pp. 2173–2183, Sep. 2000.

[20] Z. Quan, S. Cui, A. H. Sayed, and H. V. Poor, "Optimal multiband joint detection for spectrum sensing in cognitive radio networks," *IEEE Trans. Signal Process.*, vol. 57, no. 3, pp. 1128–1140, Mar. 2009.

[21] Z. Tian and G. B. Giannakis, "A wavelet approach to wideband spectrum sensing for cognitive radios," in *Proc. Int. Conf. Cogn. Radio Oriented Wireless Netw. Commun.*, Jun. 2006, pp. 1–5.

[22] B. Farhang-Boroujeny, "Filter bank spectrum sensing for cognitive radios," *IEEE Trans. Signal Process.*, vol. 56, no. 5, pp. 1801–1811, May 2008.

[23] A. Sonnenschein and P. M. Fishman, "Radiometric detection of spread-spectrum signals in noise of uncertain power," *IEEE Trans. Aerosp. Electron. Syst.*, vol. 28, no. 3, pp. 654–660, Jul. 1992.

[24] F. F. Digham, M. S. Alouini, and M. K. Simon, "On the energy detection of unknown signals over fading channels," *IEEE Trans. Commun.*, vol. 55, no. 1, pp. 21–24, Jan. 2007.

[25] P. C. Sofotasios, E. Rebeiz, L. Zhang, T. A. Tsiftsis, D. Cabric, and S. Freear, "Energy detection based spectrum sensing over $\kappa-\mu$ and $\kappa-\mu$ extreme fading channels," *IEEE Trans. Veh. Technol.*, vol. 62, no. 3, pp. 1031–1040, Mar. 2013.

[26] H. V. Poor, *An Introduction to Signal Detection and Estimation*. New York, NY, USA: Springer-Verlag, 1994.

[27] W. A. Gardner, "Signal interception: a unifying theoretical framework for feature detection," *IEEE Trans. Commun.*, vol. 36, no. 8, pp. 897–906, Aug. 1988.

[28] C. Guo, S. Chen, and F. Liu, "Polarization-based spectrum sensing algorithms for cognitive radios: Upper and practical bounds and experimental assessment," *IEEE Trans. Veh. Technol.*, vol. 65, no. 10, pp. 8072–8086, Oct. 2016.

[29] A. Kortun, M. Sellathurai, T. Ratnarajah, and C. Zhong, "Distribution of the ratio of the largest eigenvalue to the trace of complex Wishart matrices," *IEEE Trans. Signal Process.*, vol. 60, no. 10, pp. 5527–5532, Oct. 2012.

[30] Y. Zeng and Y.-C. Liang, "Eigenvalue-based spectrum sensing algorithms for cognitive radio," *IEEE Trans. Commun.*, vol. 57, no. 6, pp. 1784–1793, Jun. 2009.

[31] Y. Zeng and Y. C. Liang, "Spectrum-sensing algorithms for cognitive radio based on statistical covariances," *IEEE Trans. Veh. Technol.*, vol. 58, no. 4, pp. 1804–1815, May 2009.

[32] P. Bianchi, M. Debbah, M. Maida, and J. Najim, "Performance of statistical tests for single-source detection using random matrix theory," *IEEE Trans. Inf. Theory*, vol. 57, no. 4, pp. 2400–2419, Apr. 2011.

[33] T. E. Bogale and L. Vandendorpe, "Moment based spectrum sensing algorithm for cognitive radio networks with noise variance uncertainty," in *Proc. Annu. Conf. on Inform. Sci. and Syst. (CISS)*, Mar. 2013, pp. 1–5.

[34] T. E. Bogale and L. Vandendorpe, "Max-min SNR signal energy based spectrum sensing algorithms for cognitive radio networks with noise variance uncertainty," *IEEE Trans. Wireless Commun.*, vol. 13, no. 1, pp. 280–290, Jan. 2014.

[35] T. E. Bogale and L. Vandendorpe, "Linearly combined signal energy based spectrum sensing algorithm for cognitive radio networks with noise variance uncertainty," in *Proc. Int. Conf. on Cognitive Radio Oriented Wireless Networks*, Jul. 2013, pp. 80–86.

[36] R. Tandra and A. Sahai, "SNR walls for signal detection," *IEEE J. Sel. Topics Signal Process.*, vol. 2, no. 1, pp. 4–17, Feb. 2008.

[37] E. H. Gismalla and E. Alsusa, "On the performance of energy detection using Bartlett's estimate for spectrum sensing in cognitive radio systems," *IEEE Trans. Signal Process.*, vol. 60, no. 7, pp. 3394–3404, Jul. 2012.

[38] E. Yousif, T. Ratnarajah, and M. Sellathurai, "A frequency domain approach to eigenvalue-based detection with diversity reception and spectrum estimation," *IEEE Trans. Signal Process.*, vol. 64, no. 1, pp. 35–47, Jan. 2016.

[39] S. Dikmese, P. Sofotasios, M. Renfors, and M. Valkama, "Subband energy based reduced complexity spectrum sensing under noise uncertainty and frequency-selective spectral characteristics," *IEEE Trans. Signal Process.*, vol. 64, no. 1, pp. 131–145, Jan. 2016.

[40] A. A. A. Boulogeorgos, N. D. Chatzidiamantis, and G. K. Karagiannidis, "Energy detection spectrum sensing under RF imperfections," *IEEE Trans. Commun.*, vol. 64, no. 7, pp. 2754–2766, Jul. 2016.

[41] A. A. A. Boulogeorgos, N. D. Chatzidiamantis, and G. K. Karagiannidis, "Spectrum sensing with multiple primary users over fading channels," *IEEE Commun. Lett.*, vol. 20, no. 7, pp. 1457–1460, Jul. 2016.

[42] A. Patel, S. Biswas, and A. K. Jagannatham, "Optimal GLRT-based robust spectrum sensing for MIMO cognitive radio networks with CSI uncertainty," *IEEE Trans. Signal Process.*, vol. 64, no. 6, pp. 1621–1633, Mar. 2016.

[43] Q. Huang and P. J. Chung, "An F–test based approach for spectrum sensing in cognitive radio," *IEEE Trans. Wireless Commun.*, vol. 12, no. 8, pp. 4072–4079, Aug. 2013.

[44] A. Taherpour, M. Nasiri-Kenari, and S. Gazor, "Multiple antenna spectrum sensing in cognitive radios," *IEEE Trans. Wireless Commun.*, vol. 9, no. 2, pp. 814–823, Feb. 2010.

[45] P. Wang, J. Fang, N. Han, and H. Li, "Multiantenna-assisted spectrum sensing for cognitive radio," *IEEE Trans. Veh. Technol.*, vol. 59, no. 4, pp. 1791–1800, May 2010.

[46] E. Biglieri, R. Calderbank, A. Constantinides, A. Goldsmith, A. Paulraj, and H. V. Poor, *MIMO Wireless Communications*. New York, NY, USA: Cambridge Univ. Press, 2007.

[47] T. M. Getu, W. Ajib, and R. Jr. Landry, "Simple F–test based spectrum sensing techniques for multi-antenna cognitive radios," *IEEE Trans. Commun.*, Jun. 2018, accepted.

[48] B. Song, M. Haardt, and F. Roemer, "A tensor-based subspace method for blind estimation of MIMO channels," in *Proc. Int. Symp. on Wireless Commun. Syst. (ISWCS)*, Aug. 2013, pp. 1–5.

[49] J. R. Magnus and H. Neudecker, *Matrix Differential Calculus With Applications in Statistics and Econometrics*, 3rd ed. Hoboken, NJ, USA: Wiley, 2007.

[50] D. Ramírez, J. Vía, I. Santamaría, and L. L. Scharf, "Detection of spatially correlated Gaussian time series," *IEEE Trans. Signal Process.*, vol. 58, no. 10, pp. 5006–5015, Oct. 2010.

[51] D. Cabric, "Addressing feasibility of cognitive radios," *IEEE Signal Process. Mag.*, vol. 25, no. 6, pp. 85–93, Nov. 2008.